Reciprocating propagation of laser pulse intensity in free space

Zhaoyang Li (zhaoyang-li@ile.osaka-u.ac.jp)
Osaka University https://orcid.org/0000-0002-2851-6506
Yanjun Gu
Osaka University
Junji Kawanaka
Osaka University https://orcid.org/0000-0001-5655-7981

Article

Keywords: free space, laser pulse intensity, constant-speed straight-line propagation. Rayleigh length

Posted Date: February 8th, 2021

DOI: https://doi.org/10.21203/rs.3.rs-171174/v1

Version of Record: A version of this preprint was published at Communications Physics on May 4th, 2021. See the published version at https://doi.org/10.1038/s42005-021-00590-8.

Reciprocating propagation of laser pulse intensity in free space

Zhaoyang Li,* Yanjun Gu, and Junji Kawanaka

Institute of Laser Engineering, Osaka University, 2-6 Yamada-oka, Suita, Osaka 565-0871, Japan

*zhaoyang-li@ile.osaka-u.ac.jp

The constant-speed straight-line propagation in free space is a basic characteristic of light. Recently, several novel spatiotemporal coupling methods, for example flying focus (or named sliding focus), are developed to control light propagation including velocity and direction. In the method of flying focus, where temporal chirp and longitudinal chromatism are combined to increase the degree of freedom for coherent control, tunable-velocities and even backward-propagation have been demonstrated. Herein, we studied the transverse and longitudinal effects of the flying focus in space and time, respectively, and found in a specific physics interval existing an unusual reciprocating propagation that was quite different from the previous result. By significantly increasing the Rayleigh length in space and the temporal chirp in time, the newly created flying focus can propagate along a longitudinal axis firstly forward, secondly backward, and lastly forward again, and the longitudinal spatial resolution for a clear reciprocation flying focus improves with increasing the temporal chirp. When this new type of light is applied in the radiation pressure experiment, a reciprocating radiation-force can be produced in space-time accordingly. This finding further extends the control of light and might enable important potential applications.

Introduction

Optical pulse propagation, including velocity and direction, is a very basic characteristic for applications like optical information/communication, laser-matter interaction, and so on [1-6]. In linear physics, an optical pulse propagates along a straight-line trajectory at the velocity of c/n, where c is the speed of light in the vacuum and n is the refractive index of the medium. In this case, the propagation velocity and/or direction can be controlled by crafting the spectrum- and space-dependent refractive index [7-12]. However, this kind of method cannot be directly applied in free space, where the refractive index is constant $n = 1$. Another approach is by shaping beam in space or pulse in time to change the propagation velocity (e.g., superluminal or accelerating velocity) and direction (e.g., straight-line or bended trajectory) in free space [13-23]. For example, a Bessel beam can propagate along a straight-line trajectory at a superluminal velocity governed by $c/\cos\alpha$ in free space, where α is the half conical angle of the conical superposition [13, 14]; an Airy beam can propagate along a parabolic trajectory at an accelerating superluminal group velocity in free space [15-22]; an Airy-Bessel pulsed beam (called light bullet) can propagate along a straight-line trajectory at an accelerating superluminal group velocity in a dispersion medium [23].

Currently, the spatiotemporal (ST) coupling is frequently used to modulate the propagation or structure of a pulsed beam, which permits both velocity control (i.e., superluminal or subluminal, and accelerating or decelerating) and direction control (i.e., forward or backward) [24-38]. The first example is the 3-dimensional (3-D) flying focus (FLFO) within the extended Rayleigh length independently demonstrated by Quéré, *et al*. [24, 25] (originally named "sliding focus") and Froula, *et al*. [26, 27] (originally named "flying focus"), respectively, which can propagate at an arbitrary group velocity in free space including all motion forms of superluminal or subluminal, accelerating or decelerating, and forward or backward propagations. The second example is the 2-D optical ST wave-packet demonstrated by Abouraddy, *et al*. [28-34], which can also propagate at an arbitrary group velocity in free space including all above motion forms. The third example is the 3-D ST Gauss-Bessel pulsed-beam (or 3-D optical wave-packet) created by pre-deforming the pulse-front of the input Gauss pulsed-beam that is for the generation of a Gauss-Bessel pulsed-beam [35, 36], similarly whose group velocity is tunable, too. Apart from the above motion forms (i.e., superluminal or subluminal, accelerating or decelerating, and forward or backward propagations), a compound motion with several different motion forms in a single propagation path is also possible [36].

In the above methods, we can find that the created optical pulse/wave-packet can only propagate towards one certain direction (i.e., forward or backward), although the propagation velocity (i.e., superluminal or subluminal, and accelerating or decelerating) and trajectory (i.e., straight-line or bend) can be well controlled. In this article, we report a new phenomenon of a reciprocation FLFO, whose motion form includes three steps: forward-propagation firstly, backward-propagation secondly, and forward-propagation again lastly. For the FLFO created by longitudinal chromatism and temporal chirp [24, 26], whose group velocity within the extended Rayleigh length has been well studied under the geometry optics, however the influence of the Rayleigh length that determined by the F-number is not well considered. Here, we significantly increase the Rayleigh length with respect to the focus-separation induced by longitudinal chromatism and then compare the propagation dynamics of the FLFO with the previous case. The result shows, the FLFO experiences a forward-backward-forward reciprocating propagation from the appearance to

the disappearance. This unusual motion of the reciprocation FLFO may bring new potentials in applications like, particle manipulation, laser acceleration, radiation generation, and so on. In this article, we took the nanoparticle ultrafast trapping or manipulation as an example and analyzed the ST-variable radiation-force induced by this reciprocation FLFO, which may bring new opportunities to this field.

Results and discussion

Generation mechanism. Figure 1a shows the schematic of the FLFO that frequently appears in an ultrafast optical experiment. Before the iris diaphragm [not shown in Fig. 1a], the pulse duration is stretched by a dispersion material (e.g., bulk material or fiber) with positive chirp in time, and the multi-spectral wave-fronts are deformed by a chromatic-aberration telescope (e.g., confocal transmission telescope only for the center frequency) with normal dispersion in space. The result is the low-frequency component is flying at the temporal leading edge and is focused onto the location far away from the focusing lens, vice versa. The propagation of this FLFO has already been well studied, and the velocity equation has been derived by Quéré, *et al*. [24, 25] and Froula, *et al*. [26, 50] independently. If based on geometrical optics and linear approximation, the velocity equation can be simplified as

$$\upsilon_{FLFO} \approx \frac{-z_f}{z_c - z_f} c \,, \tag{1}$$

where, z_c and z_f are temporal chirp and longitudinal chromatism induced longitudinal pulse-separation and focus-separation, respectively, which corresponds to the pulse bandwidth $\Delta\omega$, and c is the light speed in free space. When $z_c/z_f > 1$ (i.e., $z_c > z_f > 0$ for the case of positive temporal chirp and normal spatial dispersion that is the case in this article, or $z_c < z_f < 0$ for the case of negative temporal chirp and abnormal spatial dispersion), the result of Eq. (1) is negative, showing a backward-propagation FLFO [see Fig. 1d]. The mechanism of the velocity control is that the longitudinal chromatism spatially separates the frequency-dependent focuses on the propagation axis and the temporal chirp temporally controls the time of every frequency arriving at its focus, resulting in a moving pulse-intensity-peak (i.e., FLFO). Figure 1b schematically shows: at time t_1, both low- and high-frequencies are before their geometrical focuses, and no FLFO exists; at time t_2, the low-frequency arrives at its geometrical focus, while the high-frequency doesn't (due to $z_c > z_f > 0$), and the FLFO appears at the ST position of the low-frequency; at time t_3, the low-frequency has passed through its geometrical focus, while the high-frequency is now at its geometrical focus (due to $z_c > z_f > 0$), and the FLFO flies backwards to the ST position of the high-frequency; finally at time t_4, both low- and high-frequencies have passed through their geometrical focuses, and the FLFO disappears. During this process, all frequencies move forwards at the light speed in free space c, but the FLFO flies backwards at the velocity governed by Eq. (1), which can be superluminal or subluminal. Figure 1d shows the dependence of the velocity of this FLFO with the temporal chirp induced pulse-separation z_c that is normalized by the longitudinal chromatism induced focus-separation z_f.

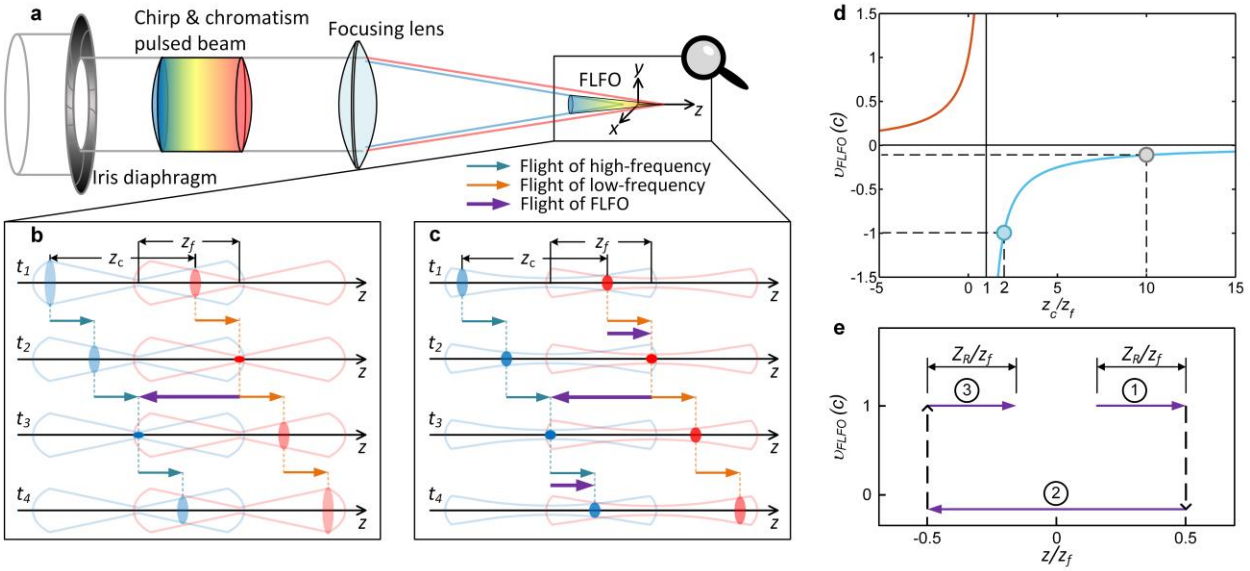

Fig. 1. Generation mechanism and characteristic of reciprocation flying focus (FLFO). a FLFO is formed by coupling of longitudinal chromatism and temporal chirp within an extended Rayleigh length. Longitudinal chromatism separates frequency-dependent focuses in space, and

temporal chirp controls moments of frequencies arriving at their focuses in time, resulting in a moving pulse-intensity-peak, i.e., a velocity tunable FLFO. **b** Typical backward-propagation FLFO with short Rayleigh lengths, at time t_1 all frequencies are before their focuses; at time t_2 low-frequency arrives at its focus, while high-frequency doesn't; at time t_3 high-frequency arrives at its focus, while low-frequency leaves its focus; at time t_4 all frequencies leave their focuses. FLFO moves backwards from the focus of low-frequency to that of high-frequency from time t_2 to t_3. z_c and z_f are temporal chirp and longitudinal chromatism induced on-axis pulse-separation and focus-separation corresponding to the pulse bandwidth, respectively. Here $z_c > z_f > 0$ with positive temporal chirp and normal spatial dispersion, i.e., low-frequency locates at the temporal leading edge and has a long focal length. **c** Reciprocation FLFO with enlarged Rayleigh lengths, at time t_1 low-frequency enters its Rayleigh length, while high-frequency doesn't; at time t_2 low-frequency arrives at its geometrical focus, while high-frequency doesn't; at time t_3 high-frequency arrives at its geometrical focus, while low-frequency leaves its geometrical focus; at time t_4 high-frequency is still in its Rayleigh length, while low-frequency leaves its Rayleigh length. FLFO moves forwards within the low-frequency's Rayleigh length from time t_1 to t_2, backwards from the geometrical focus of low-frequency to that of high-frequency from time t_2 to t_3, and finally forwards again within the high-frequency's Rayleigh length from time t_3 to t_4. **d** Group velocity of FLFO υ_{FLFO} as a function of z_c that is normalized by z_f. **e** On-axis location of reciprocation FLFO during ① forward-, ② backward-, and finally ③ forward-propagations with corresponding velocities υ_{FLFO}. The distance/position is normalized by z_f.

In the above typical FLFO, the Rayleigh length $Z_R(\omega)$ comparing with the longitudinal chromatism induced focus-separation z_f is very short and negligible [see Fig. 1b]. When dramatically increasing the Rayleigh length $Z_R(\omega)$ by reducing the beam diameter (or numerical aperture, NA) at the focusing lens, the typical backward-propagation FLFO is changed into a reciprocation FLFO. Figure 1c schematically shows: at time t_1, the low-frequency is before its geometrical focus but has entered its Rayleigh length, while the high-frequency doesn't, showing a forward-propagation FLFO; from time t_2 to t_3, it becomes the typical backward-propagation FLFO; at time t_4, the high-frequency has passed through its geometrical focus but is still within its Rayleigh length, while the low-frequency doesn't, showing a forward-propagation FLFO again. The result is the FLFO has a reciprocating motion along the propagation axis. When the origin of the propagation z-axis is defined at the midpoint of z_f (i.e., the focus of the center frequency ω_0 for linear longitudinal chromatism), Fig. 1e shows the propagation of the reciprocation FLFO is divided into three steps: firstly, forward-propagation from $z = z_f/2 - Z_R$ to $z = z_f/2$; secondly, backward-propagation from $z = z_f/2$ to $z = -z_f/2$; thirdly, forward-propagation from $z = -z_f/2$ to $z = -z_f/2 + Z_R$. The two forward-propagations have a constant velocity c in free space, but the backward-propagation has a tunable velocity governed by Eq. (1) and shown by Fig. 1d. Here, because a limited bandwidth $\Delta\omega$ is considered, the frequency-dependence of the Rayleigh lengths $Z_R(\omega)$ is neglected, and then $Z_R(\omega)$ is represented by Z_R.

Numerical demonstration. The numerical demonstration is carried out by using the model given in the "Methods" section and the following parameters: the pulse has an 800 nm center wavelength and a 20 nm flat-top bandwidth; the focusing lens has a 400 mm (for 800 nm) focal length; the BK7 confocal telescope $f_1 - f_2$ for longitudinal chromatism introduces $z_f = 5$ mm focus-separation (for 790 ~ 810 nm), when $f_1 = f_2 = 50$ mm (for 800 nm). The temporal chirp (i.e., z_c) is modulated for FLFOs with different velocities and longitudinal spatial resolutions, and the beam diameter is adjusted by the iris diaphragm for different Rayleigh lengths Z_R. When the temporal chirp induced pulse-separation z_c is 10 mm ($2z_f$) and the Rayleigh length Z_R is 50 μm ($0.01z_f$), Fig. 2a shows the time-integrated extended Rayleigh length within a 0.1 mm × 12 mm lateral region, and Fig. 2b gives the dynamics at different propagation times t, showing a typical backward-propagation FLFO. The propagation time t in this article is defined as $t = z/c$, and the moment of the center frequency ω_0 (or the FLFO for linear temporal chirp and linear longitudinal chromatism) arriving at the space origin $z = 0$ (or the focus of the center frequency ω_0 for linear longitudinal chromatism) is the propagation time origin $t = 0$. Remaining the temporal chirp unchanged, when the Rayleigh length is enlarged to 0.75 mm ($0.15z_f$) by reducing the beam diameter from 57.2 mm to 14.8 mm, Fig. 2c shows the time-integrated extended Rayleigh length is stretched and thickened. Figure 2d shows the corresponding dynamics at different propagation times t, and the reciprocating motion of the FLFO can be found. Next, keeping the enlarged Rayleigh length ($0.15z_f$) unchanged, when the temporal chirp induced pulse-separation z_c is increased from 10 mm ($2z_f$) to 50 mm ($10z_f$) by increasing the temporal chirp, the time-integrated extended Rayleigh length remains unchanged [see Fig. 2e], however the longitudinal spatial resolution of the FLFO is enhanced, showing a clear reciprocation FLFO [see Fig. 2f]. Figure 2 indicates two results: first, increasing the Rayleigh length (by reducing NA) is necessary for the reciprocation FLFO [see Fig. 2d]; second, dramatically increasing the temporal chirp can enhance the longitudinal spatial resolution of the reciprocation FLFO [see Fig. 2f]. The previous results show a large temporal chirp would reduce the velocity of the backward-propagation. The blue and gray spots in Fig. 1d show the backward-propagation velocities in Figs. 2b/d and 2f are $-c$ and $-0.11c$, respectively, which is why the time interval during the backward-propagation in Fig. 2f is increased.

In summary, to generate a reciprocation FLFO: firstly, the temporal chirp induced pulse-separation should be longer than the longitudinal chromatism induced focus-separation $z_c/z_f > 1$ (i.e., $z_c > z_f > 0$ for the case of positive temporal chirp and normal spatial dispersion that is the case in this article, or $z_c < z_f < 0$ for the case of negative temporal chirp and abnormal spatial dispersion), generating a typical backward-propagation FLFO; secondly, the

Rayleigh length Z_R should be obviously enlarged $Z_R >> 0$, showing obvious forward-propagation FLFOs before and after the backward-propagation; thirdly, the Rayleigh length should be shorter than the longitudinal chromatism induced focus-separation $|z_f| > Z_R > 0$, improving the longitudinal spatial resolution of the FLFO; finally, the temporal chirp should be significantly enhanced $z_c/z_f >> 1$, further improving the longitudinal spatial resolution for a clear reciprocation FLFO. The requirement then becomes $|z_c| >> |z_f| > Z_R >> 0$ with $z_c/z_f > 0$.

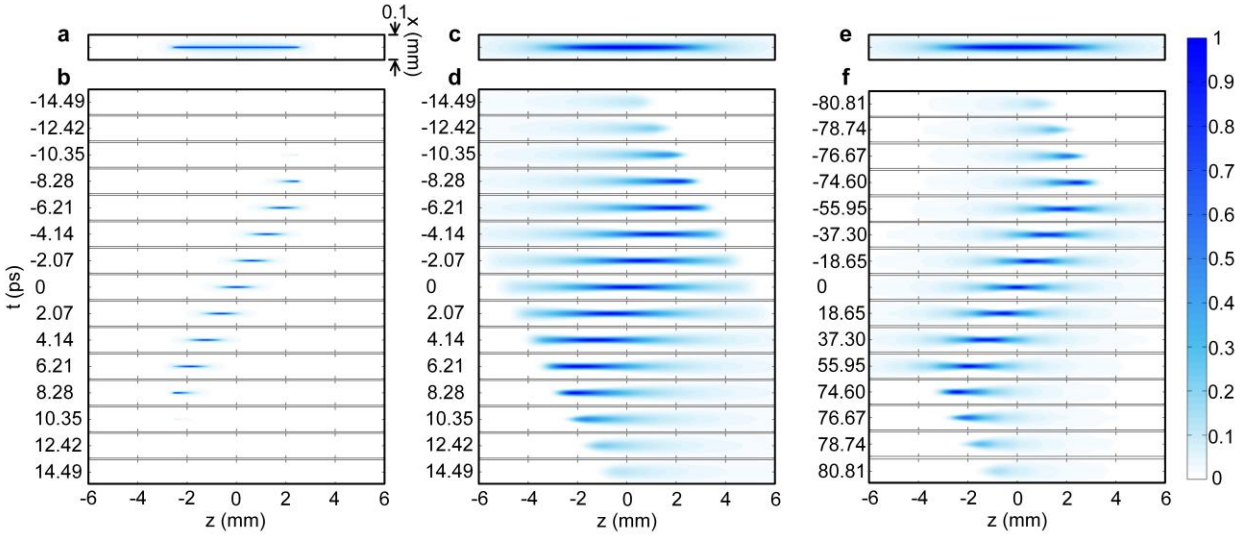

Fig. 2. Numerical demonstration and comparison. When **a, b** $Z_R = 0.01z_f$ & $z_c = 2z_f$, **c, d** $Z_R = 0.15z_f$ & $z_c = 2z_f$, and **e, f** $Z_R = 0.15z_f$ & $z_c = 10z_f$, **a, c, e** time-integrated extended Rayleigh length within a 0.1 mm × 12 mm 2-D lateral spatial region. **b, d, f** Dynamics of flying focus (FLFO) within the same 2-D lateral spatial region at different propagation times t, showing **b** typical backward-propagation FLFO, **d** reciprocation FLFO, and **f** clear reciprocation FLFO, respectively. Z_R is the Rayleigh length of the center frequency. z_c and z_f are temporal chirp and longitudinal chromatism induced on-axis pulse-separation and focus-separation corresponding to the pulse bandwidth, respectively, and $z_f = 5$ mm.

Existence of clear reciprocation FLFO. The analytical formulas given in the "Methods" section [see Eqs. (14) and (15)] show the longitudinal width (the full width at half maximum, FWHM) Δz of the reciprocation FLFO is proportional to a product $M \cdot Z_R$, i.e., $\Delta z \propto M \cdot Z_R$, where $M = z_c/(z_c - z_f)$. When the longitudinal spatial resolution of the FLFO is defined as the ratio between the FLFO longitudinal width and the longitudinal chromatism induced focus-separation $\Delta z/z_f$, the longitudinal spatial resolution of the FLFO improves with increasing the temporal chirp z_c (or with reducing the parameter M), and this agrees well with the simulation results in Figs. 2d and 2f. Figure 3 shows the temporal chirp z_c/z_f (normalized by z_f) determines both the backward-propagation velocity and the longitudinal spatial resolution of the FLFO. When the normalized temporal chirp z_c/z_f is larger than 10 [$z_c/z_f = 10$ is the case in Fig. 2f], the parameter M approaches infinitely to its minimum value 1, generating a clear reciprocation FLFO with almost the shortest longitudinal width or with almost the highest longitudinal spatial resolution. However, the backward-propagation velocity of the FLFO is limited less than $0.11c$ in free space, which would further decrease with increasing the temporal chirp z_c/z_f. Noting that, the forward-propagation velocity of the FLFO will not be affected by adjusting the temporal chirp, which always is constant c in free space. Finally, the result is that a clear reciprocation FLFO exists in the interval of $z_c/z_f \in [10, \infty)$, where it has a $[-0.11c, 0)$ subluminal backward-propagation velocity and a light-speed c forward-propagation velocity in free space. This phenomenon can be found in the simulated dynamics as shown in Fig. 2f. Another parameter affecting the longitudinal spatial resolution of the reciprocation FLFO is the Rayleigh length Z_R, which generally cannot be too small (reducing the forward-propagation distance) or too large (depredating the longitudinal spatial resolution), and the simulation here indicates it is better to keep it within around $0.1z_f \sim 0.2z_f$.

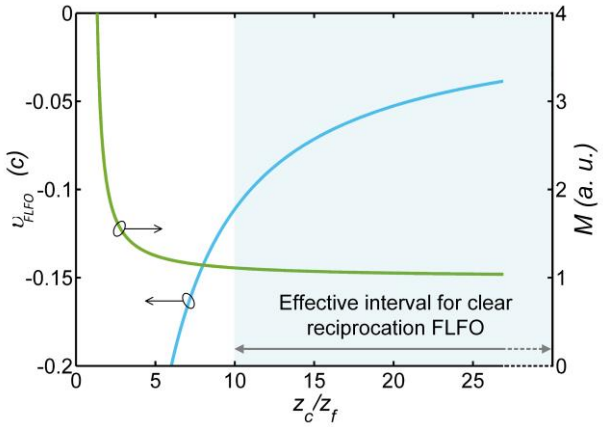

Fig. 3. Existence interval of clear reciprocation flying focus (FLFO). Group velocity of backward-propagation FLFO v_{FLFO} and parameter M as functions of z_c that is normalized by z_f. z_c and z_f are temporal chirp and longitudinal chromatism induced longitudinal pulse-separation and focus-separation corresponding to the pulse bandwidth, respectively. M equals $z_c/(z_c - z_f)$ and is proportional to the longitudinal width of the reciprocation FLFO.

Possible applications. The unique propagation form of the reciprocation FLFO provides a new tool for laser pulse intensity control in space-time. For applications like optical trapping/manipulating/accelerating small particles with the laser radiation pressure developed by Ashkin *et al*., especially in biology, medicine, and nanoscience [39-43], the dynamic radiation-force induced by the reciprocation FLFO may bring new possibilities. In the Rayleigh scattering regime where the particle is sufficiently smaller than the laser wavelength, Fig. 4a shows the radiation force exerted on a small dielectric sphere (treated as an induced, simple point dipole) can be divided into two components: a scattering force F_{scat} and a gradient force F_{grad} [42, 44]. The scattering force F_{scat} is proportional to the product $a^6 I$ and points in the direction of the beam, and the gradient force F_{grad} is proportional to the product $a^3 \nabla I$ and points in the direction of the intensity gradient, where a is the radius of the sphere and I is the laser intensity. Recently, pulsed Gaussian beams also are used as optical tweezers which can produce much stronger radiation forces than those by continuous-wave Gaussian beams [45, 46]. A study on the instantaneous radiation forces produced by the pulsed Gaussian beams shows that, for long pulses (typically longer than 1 ps), stable optical trapping/manipulation like by the continuous-wave Gaussian beams can be obtained [47]. Figure 2f shows, because both the temporal chirp and the Rayleigh length are enlarged for a clear reciprocation FLFO, the temporal length of the reciprocation FLFO is around 5 ps (much longer than 1 ps), and consequently the induced radiation forces F_{scat} and F_{grad} can be described well by the steady-state model given in the "Methods" section. Figure 4b schematically illustrates the FLFO experiences a reciprocating propagation trajectory within the extended Rayleigh length, in theory, which can produce a reciprocating radiation force in space-time. Based on the clear reciprocation FLFO shown in Fig. 2f, the induced radiation force is simulated. Figure 4c shows the spectrum of the input pulsed beam, and Fig. 4d shows the on-axis intensity distribution of the FLFO at different propagation times from its appearance (at around $t = -83$ ps) to its disappearance (at around $t = 83$ ps). Because of the subluminal velocity of the backward-propagation, the scale of the time axis (vertical axis) of Fig. 4d from $t = -75$ ps to $t = 75$ ps is reduced. When the total input energy is 1 mJ and the relative refractive index is $m = 1.511/1$, for a dielectric sphere radius $a = 2$ nm, Fig. 4e shows the on-axis gradient forces F_{grad}, scattering force F_{scat}, and net force F_{net} at the propagation time $t = 0$. The gradient force is significantly stronger than the scattering force, and the sphere can be trapped at the position $z = 0$ by the net force. Figure 4f shows the dynamics of the on-axis net force F_{net} at different propagation times from the appearance (at around $t = -83$ ps) to the disappearance (at around $t = 83$ ps), showing an ultrafast reciprocating trapping force. When the radius of the dielectric sphere is increased to $a = 10$ nm, Figs. 4g and 4h show the on-axis radiation forces at the propagation time $t = 0$ and the dynamics of the on-axis net force from $t = -83$ ps to $t = 83$ ps, respectively. The ultrafast reciprocating trapping force is now changed into an ultrafast reciprocating pushing force, because the scattering force is much larger than the gradient force that dominates the net force. The two examples given in Figs. 4f and 4h are based on small particles (dipole) and show the induced reciprocating radiation-force that may bring new possibilities to advance ultrafast optical trapping or manipulation or acceleration. Besides that, for a large particle (multipoles), because backward scattering forces exist [48], once it is combined with the reciprocation FLFO, an ultrafast reciprocating trapping force for multipoles may also be achieved.

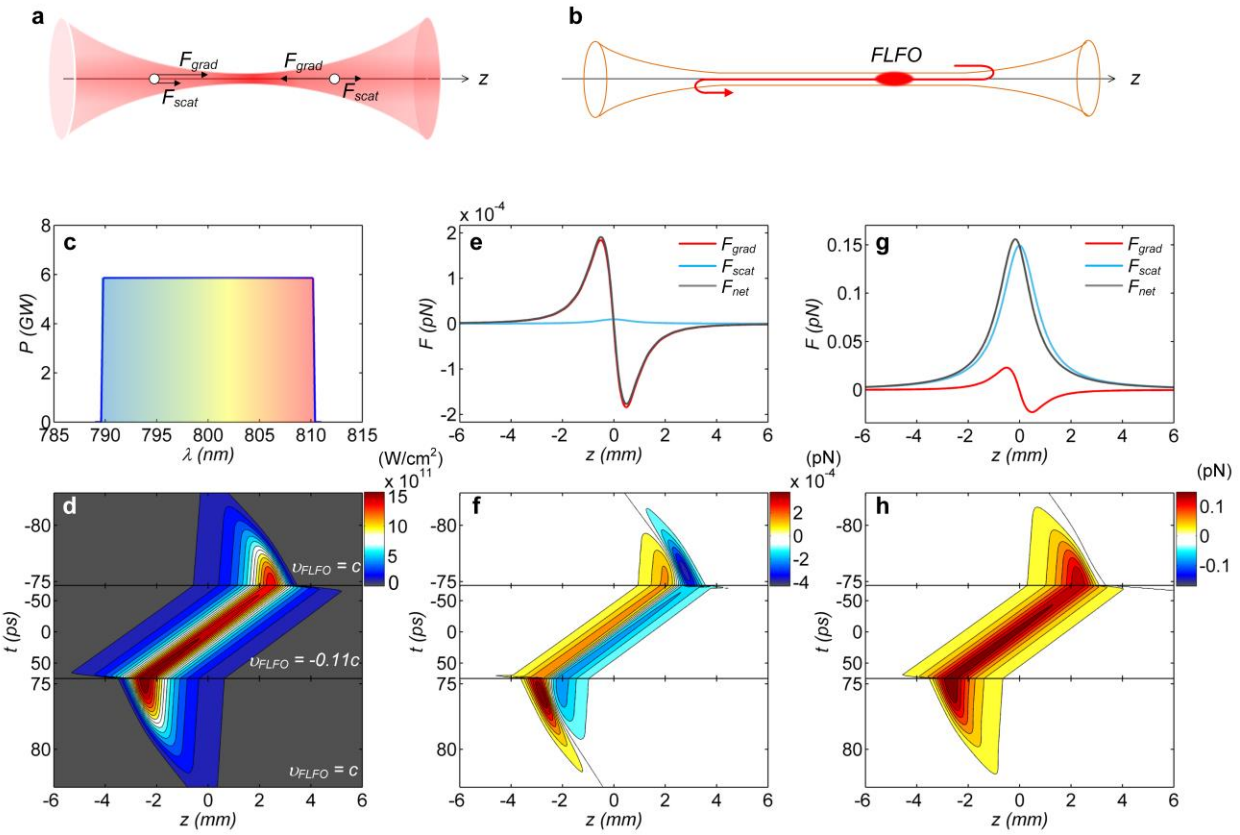

Fig. 4. Reciprocation flying focus (FLFO) induced radiation forces. a Schematic of continuous-wave Gaussian laser beam radiating a Rayleigh dielectric sphere and induced longitudinal axial (at z-axis) radiation forces of scattering force F_{scat} and gradient force F_{grad}. **b** Schematic of reciprocation FLFO in an extended Rayleigh length, and red curve illustrates the reciprocating motion trajectory. **c** Spectrum for simulation. **d** Longitudinal axial (at z-axis) intensity of FLFO at different propagation times t from appearance to disappearance, showing reciprocating propagation. Because the forward-propagation velocity c is much faster than the backward-propagation velocity -0.11c, the propagation time axis (vertical axis) is zoomed for the forward-propagation. For a very small Rayleigh dielectric sphere (2 nm radius) in the air, **e** induced longitudinal axial (at z-axis) radiation forces at the propagation time $t = 0$, and **f** induced ultrafast reciprocating trapping forces at different propagation times t from appearance to disappearance. The net force is $F_{net} = F_{grad} + F_{scat}$. For a relatively big Rayleigh dielectric sphere (10 nm radius) in the air, **g** induced longitudinal axial (at z-axis) radiation forces at the propagation time $t = 0$, and **h** induced ultrafast reciprocating pushing forces at different propagation times t from appearance to disappearance.

In addition to optical radiation pressure experiments, the ultra-intense traditional FLFO with superluminal or subluminal, accelerating or decelerating, and forward- or backward-propagation velocities recently have been used in laser-plasma physics applications like dephasingless/phase-locked laser-wakefield accelerator, arbitrary-velocity ionization wave generation, photon accelerator, laser-plasma amplifier, and so on [3-6, 26, 27, 49, 50]. The reciprocation FLFO introduced in this article, because of its new characteristics, can further enhance the controllability of the laser pulse intensity in space-time and may also provide some new opportunities in this field.

Conclusion

In this work, we have introduced a new type of laser pulse intensity propagation or a new type of optical control, i.e., the reciprocation FLFO. Based on the recently reported FLFO (or named sliding focus) that created by combining temporal chirp and longitudinal chromatism together [24-27], when both the Rayleigh length and the temporal chirp are dramatically increased, different from the previous result the produced FLFO would present an unprecedented motion form: flying forward-backward-forward along a straight-line in free space, showing a longitudinal reciprocating trajectory. The existence condition of a clear reciprocation FLFO with a high longitudinal spatial resolution is also analyzed and introduced. In free space, a clear reciprocation FLFO has a light-speed forward-propagation velocity c and a subluminal backward-propagation velocity (typically $-0.11c < v_{FLFO} < 0$), respectively. We have shown when this unique light is applied in radiation pressure experiments in the Rayleigh scattering regime, for different particle radiuses an ultrafast reciprocating trapping or pushing force can be induced in space-time. Moreover, in laser-plasma physics, the ultra-intense reciprocation FLFO can further extend the performance of the

traditional FLFO. All in all, this new type of light may provide useful and unique applications from nano-optics to high-field optics.

Methods

Numerical simulation of reciprocation FLFO. The propagation of the FLFO in a paraxial cylindrical coordinate system r-φ-z can be simulated by the Collins diffraction integral, and the optical field after an ABCD system is given by

$$E_{out}\left(r_2,\varphi_2,z,\omega\right)=-\frac{i}{\lambda B}\iint E_{in}\left(r_1,\varphi_1,z_0,\omega\right)\exp\left(ikS\right)r_1dr_1d\varphi_1\,, \tag{2}$$

with

$$S=z+\frac{1}{2B}\left[Ar_1^2-2r_1r_2\cos\left(\varphi_1-\varphi_2\right)+Dr_2^2\right], \tag{3}$$

$$\begin{bmatrix}A & B\\ C & D\end{bmatrix}=\begin{bmatrix}1 & z-z_0\\ 0 & 1\end{bmatrix}\begin{bmatrix}1 & 0\\ -\dfrac{1}{f\left(\omega\right)} & 1\end{bmatrix}, \tag{4}$$

where, $f(\omega)$ is the frequency-dependent focal length after the focusing lens, and z_0 and z is the input and output on-axis position, respectively. The input optical field is given by

$$\begin{aligned}E_{in}\left(r_1,\varphi_1,z_0,\omega\right)=A\left(\omega\right)&\exp\left[i\frac{1}{2}\phi_2\left(\omega-\omega_0\right)^2\right]\\ &\exp\left(-\frac{r_1^2}{w_{in}^2}\right)\exp\left\{-ik\left[z_0+\Delta z\left(r_1,\omega\right)\right]\right\}\end{aligned}, \tag{5}$$

where, $A(\omega)$ is the spectral amplitude, ϕ_2 is the group-velocity dispersion (GVD) denoting the temporal chirp, w_{in} is the beam waist, and $\Delta z(r_1,\omega)$ is the frequency-dependent wave-front denoting the longitudinal chromatism. For example, when a transmission telescope is used for generating the longitudinal chromatism, $\Delta z(r_1,\omega)$ is a quadratic function with respect to the transverse coordinate $\Delta z(r_1,\omega) = a(\omega)r_1^2 + b$, where $a(\omega)$ is a frequency-dependent coefficient and b is a constant-coefficient [51-54]. After the Fourier-transform, the output temporal optical field is given by

$$E_{out}\left(r_2,\varphi_2,z,\tau\right)=\frac{1}{2\pi}\int E_{out}\left(r_2,\varphi_2,z,\omega\right)\exp\left(i\omega\tau\right)d\omega\,, \tag{6}$$

where τ is the local time. By choosing different propagating positions z, the dynamics of the FLFO at different propagation times t ($t = z/c$) can be obtained. The numerical simulation can show the dynamics of FLFOs well however cannot give the mathematical influence of the Rayleigh length (i.e., normalized as Z_R/z_f) and the temporal chirp (i.e., normalized as z_c/z_f) directly. In this case, an approximately analytical formula is also required.

Analytical formula of reciprocation FLFO. In the theory of linear pulse propagation [55], a deeply chirped Gaussian pulse can be described by a complex Gaussian parameter $\Gamma = a–ib$, where, a and b here are constant coefficients denoting the pulse duration and the temporal chirp, respectively. The instantaneous frequency of this pulse at time t is $\omega(t) = \omega_0+2bt$, which shows the temporal profile of a deeply chirped Gaussian pulse can be approximately described by its spectral profile, i.e., $I(t) \propto I(\omega)$. In this case, the dynamics of a deeply chirped FLFO in space-time can be approximately described by that in space-spectrum [56].

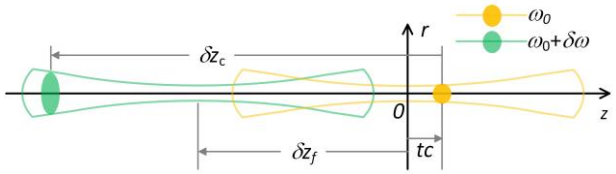

Fig. 5. Frequency-dependent propagation geometrics. Geometrical relationship among temporal chirp induced pulse-separation δz_c, longitudinal chromatism induced focus-separation δz_f, and center frequency propagating position tc. The ideal focus of the center frequency is located at the

coordinate origin $z = 0$, and the moment of the center frequency arriving at $z = 0$ is the propagation time origin $t = 0$. $\omega_0 + \delta\omega$ is an arbitrary frequency about the center frequency ω_0. The solid line and the solid spot denote Gaussian beam and frequency position, respectively.

When both temporal chirp and longitudinal chromatism are linear, an arbitrary frequency $\omega = \omega_0 + \delta\omega$ about the center frequency ω_0 has relative pulse- and focus-separations given by

$$\begin{aligned} \delta z_c &= -\frac{\delta\omega}{\Delta\omega} z_c \\ \delta z_f &= -\frac{\delta\omega}{\Delta\omega} z_f \end{aligned}, \tag{7}$$

where, $\Delta\omega$ is the bandwidth, z_c and z_f is the frequency-dependent pulse- and focus-separation corresponding to the pulse bandwidth $\Delta\omega$, respectively, and the negative sign on the right side indicates a low-frequency is at the temporal leading edge (positive temporal chirp) and has a long focus location (normal spatial dispersion). Figure 5 shows in the lateral plane of the coordinate system r-z, the space origin $z = 0$ is at the geometrical focus of the center frequency ω_0, and the propagation time origin $t = 0$ is the moment of the center frequency ω_0 arriving at the space origin, i.e., $t = z/c$. The longitudinal chromatism moves the geometrical focus (waist) of an arbitrary frequency $\omega = \omega_0 + \delta\omega$ to the position $z_{gf}(\omega)$, which is only frequency-dependent. At the propagation time t, the temporal chirp moves the instantaneous location of an arbitrary frequency $\omega = \omega_0 + \delta\omega$ to the position $z_{il}(\omega,t)$, which is both frequency- and time-dependent. The values of these two positions are given by

$$\begin{aligned} z_{gf}(\omega) &= \delta z_f \\ z_{il}(\omega,t) &= tc + \delta z_c \end{aligned}. \tag{8}$$

From the simultaneous Eqs. (7) and (8), an arbitrary frequency $\omega = \omega_0 + \delta\omega$ arrives at its geometrical focus at the propagation time

$$t_{gf}(\omega) = \frac{z_c - z_f}{c}\frac{\delta\omega}{\Delta\omega}. \tag{9}$$

Then, the approximately analytical formula governing the propagation dynamics of a deeply chirped Gaussian FLFO is given by

$$I(r,\omega,t) = I_0(\omega)\frac{w_0^2(\omega)}{w_z^2(\omega,t)}\exp\left[-2\frac{r^2}{w_z^2(\omega,t)}\right], \tag{10}$$

with

$$w_z(\omega,t) = w_0(\omega)\sqrt{1+\left[\frac{z_{il}(\omega,t)-z_{gf}(\omega)}{Z_R(\omega)}\right]^2}, \tag{11}$$

$$Z_R(\omega) = \frac{1}{2}kw_0^2(\omega), \tag{12}$$

where, $I_0(\omega)$ is the spectral intensity, $w_0(\omega)$ is the beam waist equaling $(\omega_0/\omega)w_0$ where w_0 is that of the center frequency, $w_z(\omega,t)$ is the beam radius at the propagation time t, $Z_R(\omega)$ is the Rayleigh length, k is the wavenumber, and the propagating position $z_{il}(\omega,t)$ is a function of frequency ω and propagation time t governed by Eq. (8).

By substituting Eqs. (7) and (8) with (11) then with Eq. (10), the on-axis FLFO is simplified as

$$I(r=0,\omega,t) = I_0(\omega)\frac{1}{1+\left[\frac{z_{il}(\omega,t)(z_c-z_f)+tc\cdot z_f}{Z_R z_c}\right]^2}. \tag{13}$$

Figures 1c and 1e show the first forward-propagation FLFO appears when the lowest-frequency $\delta\omega = -\Delta\omega/2$ arrives at $z_{il} = z_f/2 - Z_R$, from Eq. (13) the on-axis peak intensity equals $0.5I_0(\omega_0 - \Delta\omega/2)$; the backward-propagation FLFO appears when every frequency respectively arrives at its geometrical focus from $z_{il} = z_f/2$ to $z_{il} = -z_f/2$ at the propagation time governed by Eq. (9), from Eq. (13) the on-axis peak intensity equals $I_0(\omega)$; the second forward-propagation FLFO disappears when the highest-frequency $\delta\omega = \Delta\omega/2$ arrives at $z_{il} = -z_f/2 + Z_R$, from Eq. (13) the on-axis peak intensity

also equals $0.5I_0(\omega_0+\Delta\omega/2)$. Once neglecting the spectral profile and considering a normalized case, the first forward-propagation FLFO has a position-dependent increasing peak intensity from 0.5 to 1 after the appearance; the backward-propagation FLFO has a fixed peak intensity of 1; the second forward-propagation FLFO has a position-dependent decreasing peak intensity from 1 to 0.5 before the disappearance.

When the spectral profile $I_0(\omega)$ within the extended Rayleigh length is neglected (i.e., flattop profile), which is reasonable for the case of $|z_c| >> |z_f| > Z_R >> 0$ and $z_c/z_f > 0$, Δz is defined as the FWHM longitudinal width of the FLFO. When the first forward-propagation FLFO appears at $\delta\omega = -\Delta\omega/2$ and $z_{il} = z_f/2-Z_R$, the FWHM width of the FLFO is given by

$$\Delta z = \sqrt{3}\frac{2z_c}{z_c - z_f}Z_R, \tag{14}$$

where the coefficient $\sqrt{3}$ is only for the case of $\delta\omega = -\Delta\omega/2$ and $z_{il} = z_f/2-Z_R$, which decreases during the forward propagation. The backward-propagation FLFO has a constant FWHM width that is given by

$$\Delta z = \frac{2z_c}{z_c - z_f}Z_R. \tag{15}$$

When the second forward-propagation FLFO disappears at $\delta\omega = \Delta\omega/2$ and $z_{il} = -z_f/2+Z_R$, the FWHM width of the FLFO is also given by Eq. (14).

Equations (14) and (15) show the forward-propagation FLFOs have variable longitudinal widths, which decreases and increases in the first and the second forward propagations, respectively. While Eq. (15) shows the backward-propagation FLFO has a constant longitudinal width. This result agrees well with the simulation shown in Fig. 2f. Equations (14) and (15) also show the longitudinal widths of the FLFOs are proportional to a product $M \cdot Z_R$ where $M = z_c/(z_c - z_f)$, although the values are slightly different in forward and backward propagations.

Radiation forces in the Rayleigh scattering regime. Under the zeroth-order approximation of the continuous-wave Gaussian beam or a weakly focused continuous-wave Gaussian beam, the formulas of the scattering and gradient forces F_{scat} and F_{grad} exerted on a Rayleigh dielectric sphere in a steady-state are given by [42, 44]

$$\vec{F}_{scat}(x,y,z) = \hat{z}\left(\frac{n_2}{c}\right)\frac{8}{3}\pi(ka)^4 a^2\left(\frac{m^2-1}{m^2+2}\right)^2 I(x,y,z), \tag{16}$$

and

$$\vec{F}_{grad}(x,y,z) = \frac{2\pi n_2 a^3}{c}\left(\frac{m^2-1}{m^2+2}\right)^2 \nabla I(x,y,z), \tag{17}$$

where, n_1 and n_2 are the refractive indexes of the dielectric sphere and the environment, $m = n_1/n_2$ is the relative refractive index, a is the radius of the dielectric sphere, $I(x, y, z)$ is the laser intensity, and $\nabla I(x, y, z)$ is the laser intensity gradient.

Acknowledgements

This work was supported by the JST-Mirai Program, Japan, under contract JPMJMI17A1.

Author contributions

Z.L. developed the concept, derived the equations, performed the simulations, and wrote the manuscript. Y.G. commented on the application part, and J.K. commented on the optical propagation part. All authors discussed the results and commented on the manuscript.

Competing interests

The authors declare no competing interests

References

1. Yin, X. & Zhang, X. Unidirectional light propagation at exceptional points. *Nature Mater.* **12**, 175–177 (2013).

2. Yessenov, M., Bhaduri, B., Delfyett, P. J. & Abouraddy, A, F. Free-space optical delay line using space-time wave packets. *Nat. Commun.* **11**, 5782 (2020).
3. Turnbull, D. et al. Ionization waves of arbitrary velocity. *Phys. Rev. Lett.* **120**, 225001 (2018).
4. Howard, A. J., Turnbull, D., Davies, A. S., Franke, P., Froula, D. H. & Palastro, J. P. Photon acceleration in a flying focus. *Phys. Rev. Lett.* **123**, 124801 (2019).
5. Palastro, J. P., Shaw, J. L., Franke, P., Ramsey, D., Simpson, T. T. & Froula, D. H. Dephasingless laser wakefield acceleration. *Phys. Rev. Lett.* **124**, 134802 (2020).
6. Caizergues, C., Smartsev, S., Malka, V. & Thaury, C. Phase-locked laser-wakefield electron acceleration. *Nat. Photonics* **14**, 475–479 (2020).
7. Hau, L. V., Harris, S. E., Dutton, Z. & Behroozi, C. Light speed reduction to 17 m per second in an ultracold atomic gas. *Nature* **397**, 594–598 (1999).
8. Gehring, G. M., Schweinsberg, A., Barsi, C., Kostinski, N. & Boyd, R. W. Observation of backward pulse propagation through a medium with a negative group velocity. *Science* **312**, 895–897 (2005).
9. Dolling, G., Enkrich, C., Wegener, M., Soukoulis, C. M. & Linden, S. Simultaneous negative phase and group velocity of light in a metamaterial. *Science* **312**, 892–894 (2005).
10. Baba, T. Slow light in photonic crystals. *Nat. Photonics* **2**, 465–473 (2008).
11. Boyd, R. W. & Gauthier, D. J. Controlling the velocity of light pulses. *Science* **326**, 1074–1077 (2009).
12. Simpson, T. T. et al. Nonlinear spatiotemporal control of laser intensity. *Opt. Express* **28**, 38516-38526 (2020).
13. Durnin, J., Miceli, J. J. & Eberly, J. H. Diffraction-free beams. *Phys. Rev. Lett.* **58**, 1499–1501 (1987).
14. Alexeev, I., Kim, K. Y. & Milchberg, H. M. Measurement of the superluminal group velocity of an ultrashort bessel beam pulse. *Phys. Rev. Lett.* **88**, 073901, (2002).
15. Siviloglou, G. A. & Christodoulides, D. N. Accelerating finite energy Airy beams. *Opt. Lett.* **32**, 979–981 (2007).
16. Siviloglou, G. A., Broky, J., Dogariu, A. & Christodoulides, D. N. Observation of accelerating Airy beams. *Phys. Rev. Lett.* **99**, 213901 (2007).
17. Siviloglou, G. A., Broky, J., Dogariu, A. & Christodoulides, D. N. Ballistic dynamics of Airy beams. *Opt. Lett.* **33**, 207-209 (2008).
18. Kaminer, I., Segev, M. & Christodoulides, D. N. Self-accelerating self-trapped optical beams. *Phys. Rev. Lett.* **106**, 213903 (2011).
19. Dolev, I., Kaminer, I., Shapira, A., Segev, M. & Arie, A. Experimental observation of self-accelerating beams in quadratic nonlinear media. *Phys. Rev. Lett.* **108**, 113903 (2012).
20. Kaminer, I., Bekenstein, R., Nemirovsky, J. & Segev, M. Nondiffracting accelerating wave packets of Maxwell's equations. *Phys. Rev. Lett.* **108**, 163901 (2012).
21. Schley, R., Kaminer, I., Greenfield, E., Bekenstein, R., Lumer, Y. & Segev, M. Loss-proof self-accelerating beams and their use in non-paraxial manipulation of particles' trajectories. *Nature Commun.* **11**, 261–267 (2015).
22. Efremidis, N. K., Chen, Z., Segev, M. & Christodoulides, D. N. Airy beams and accelerating waves: an overview of recent advances. *Optica* **6**, 686-701 (2019).
23. Chong, A., Renninger, W. H., Christodoulides, D. N. & Wise, F. W. Airy–Bessel wave packets as versatile linear light bullets. *Nat. Photonics* **4**, 103–106 (2010).
24. Sainte-Marie, A., Gobert, O. & Quéré, F. Controlling the velocity of ultrashort light pulses in vacuum through spatio-temporal couplings. *Optica* **4**, 1298-1304 (2017).
25. Jolly, S. W., Gobert, O., Jeandet, A. & Quéré, F. Controlling the velocity of a femtosecond laser pulse using refractive lenses. *Opt. Express* **28**, 4888-4897 (2020).
26. Froula, D. H., et al. Spatiotemporal control of laser intensity. *Nat. Photonics* **12**, 262-265 (2018).
27. Froula, D. H., et al. Flying focus: Spatial and temporal control of intensity for laser-based applications. *Phys. Plasmas* **26**, 032109 (2019).
28. Kondakci, H. E. & Abouraddy, A. F. Diffraction-free space-time beams. *Nat. Photonics* **11**, 733–740 (2017).
29. Kondakci, H. E. & Abouraddy, A. F. Airy wavepackets accelerating in space-time. *Phys. Rev. Lett.* **120**, 163901 (2018).
30. Bhaduri, B., Yessenov, M. & Abouraddy, A. F. Meters-long propagation of diffraction-free space-time light sheets. *Opt. Express* **26**, 20111–20121 (2018).
31. Kondakci, H. E. & Abouraddy, A. F. Optical space-time wave packets having arbitrary group velocities in free space. *Nat. Commun.* **10**, 929 (2019).
32. Bhaduri, B., Yessenov, M. & Abouraddy, A. F. Space-time wave packets that travel in optical materials at the speed of light in vacuum. *Optica* **6**, 139-146 (2019).
33. Yessenov, M. & Abouraddy, A. F. Changing the speed of optical coherence in free space. *Opt. Lett.* **44**, 5125-5128 (2019).
34. Yessenov, M. & Abouraddy, A. F. Accelerating and decelerating space-time optical wave packets in free space. *Phys. Rev. Lett.* **125**, 233901 (2020).
35. Li, Z. & Kawanaka, J. Velocity and acceleration freely tunable straight-line propagation light bullet. *Sci. Rep.* **10**, 11481 (2020).
36. Li, Z. & Kawanaka, J. Optical wave-packet with nearly-programmable group velocities. *Commun. Phys.* **3**, 211 (2020).
37. Valtna, H., Reivelt, K. & Saari, P. Methods for generating wideband localized waves of superluminal group velocity. *Opt. Comm.* **278**, 1–7 (2007).
38. Li, Z. & Miyanaga, N. Theoretical method for generating regular spatiotemporal pulsed-beam with controlled transverse-spatiotemporal dispersion. *Opt. Commun.* **432**, 91-96 (2019).
39. Ashkin, A. Acceleration and trapping of particles by radiation pressure. *Phys. Rev. Lett.* **24**, 156-159 (1970).
40. Ashkin, A. Tapping of atoms by resonance radiation pressure. *Phys. Rev. Lett.* **40**, 729-732 (1978).
41. Ashkin, A. Applications of laser radiation pressure. *Science* **210**, 4474 (1980).
42. Ashkin, A., Dziedzic, J. M., Bjorkholm, J. E. & Chu, S. Observation of a single-beam gradient force optical trap for dielectric particles. *Opt. Lett.* **11**, 288-290 (1986).
43. Ashkin, A. Optical trapping and manipulation of neutral particles using lasers. *Proc. Natl. Acad. Sci. U.S.A.* **94**, 4853-4860 (1997).
44. Harada, Y. & Asakura, T. Radiation forces on a dielectric sphere in the Rayleigh scattering regime. *Opt. Commun.* **124**, 529-541 (1996).
45. Ambardekar, A. A. & Li, Y. Q. Optical levitation and manipulation of stuck particles with pulsed optical tweezers. *Opt. Lett.* **30**, 1797-1799 (2005).
46. Deng, J. L., Wei, Q., Wang, Y. Z. & Li, Y. Q. Numerical modeling of optical levitation and trapping of the stuck particles with a pulsed optical tweezers. *Opt. Express* **13**, 3673-3680 (2006).

47. Wang, L.-G. & Zhao, Ch.-L. Dynamic radiation force of a pulsed Gaussian beam acting on a Rayleigh dielectric sphere. *Opt. Express* **15**, 10615-10621 (2007).
48. Chen, J., Ng, J., Lin, Z. & Chan, C. T. Optical pulling force. *Nat. Photonics* **5**, 531-534 (2011).
49. Turnbull, D. et al. Flying focus and its application to plasma-based laser amplifiers. *Plasma Phys. Control. Fusion* **61**, 014022 (2018).
50. Franke, P. et al. Measurement and control of large diameter ionization waves of arbitrary velocity. *Opt. Express* **27**, 31978-31988 (2019).
51. Bor, Z. Distortion of femtosecond laser pulses in lenses and lens systems. *J. Mod. Opt.* **35**, 1907–1918 (1988).
52. Bor, Z. Distortion of femtosecond laser pulses in lenses. *Opt. Lett.* **14**, 119–121 (1989).
53. Li, Z. & Kawanaka, J. Efficient method for determining pulse-front distortion in an ultra-intense laser. *J. Opt. Soc. Am. B* **37**, 2595-2603 (2020).
54. Jolly, S. W., Gobert, O. & Quéré, F. Spatio-temporal characterization of ultrashort laser beams: a tutorial. *J. Opt.* **22**, 103501 (2020).
55. Siegman, A. E., Lasers (University Science Books, 1986), Chap. 9.
56. Chong, A., Kuznetsova, L. & Wise, F. W. Theoretical optimization of nonlinear chirped-pulse fiber amplifiers. *J. Opt. Soc. Am. B* **24**, 1815-1823 (2007).

Figures

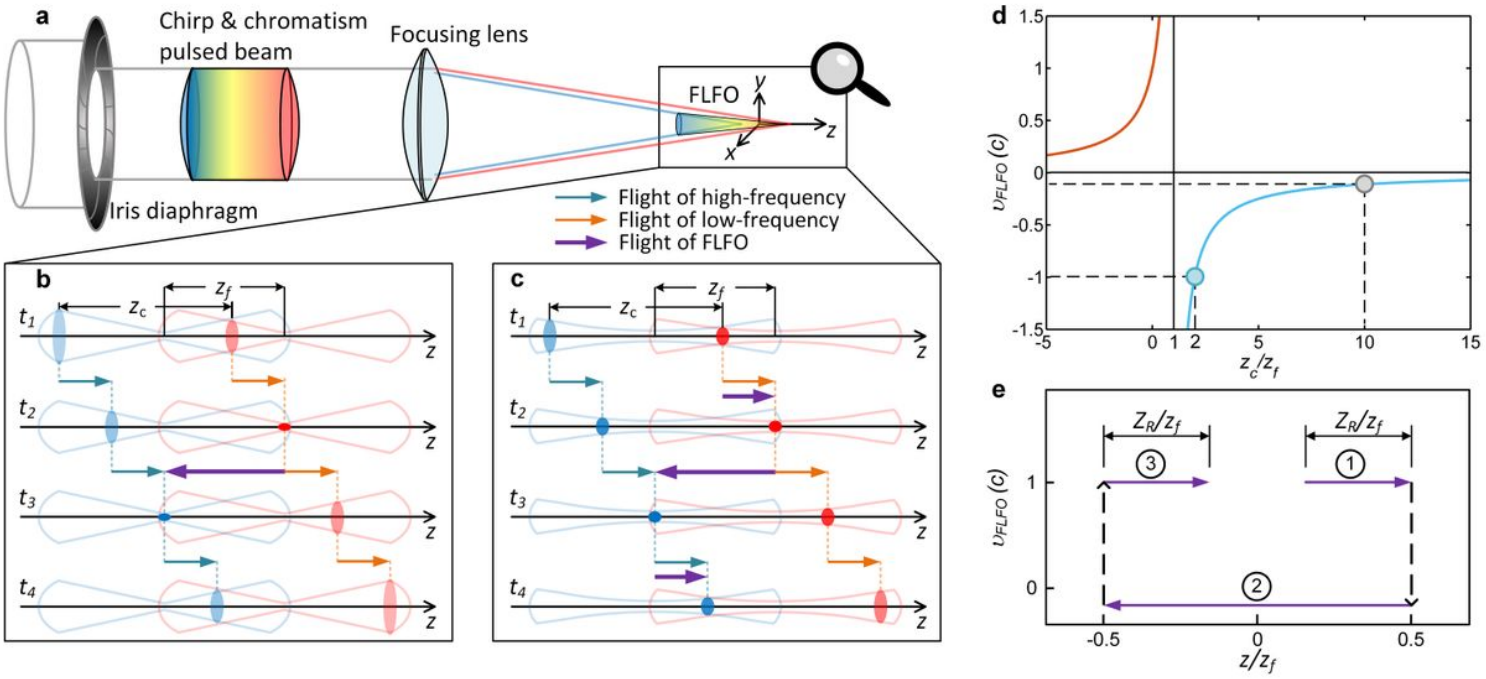

Figure 1

See manuscript for full figure caption.

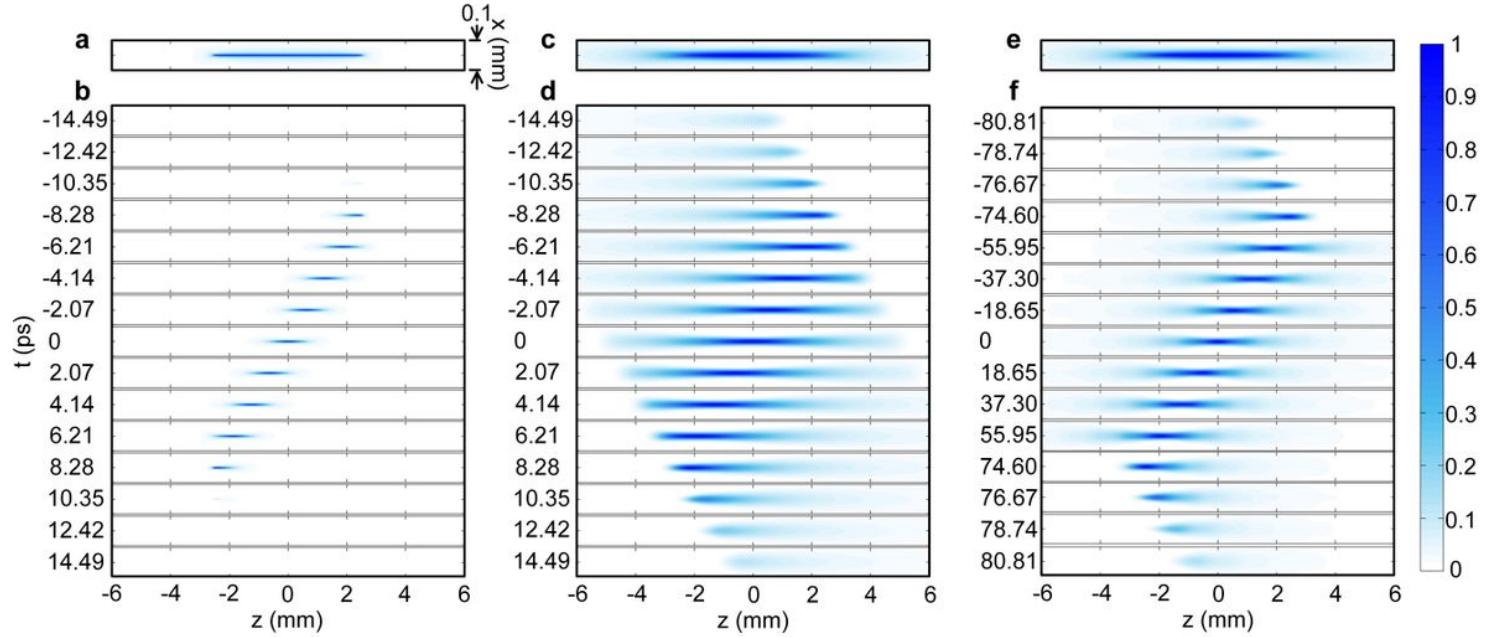

Figure 2

See manuscript for full figure caption.

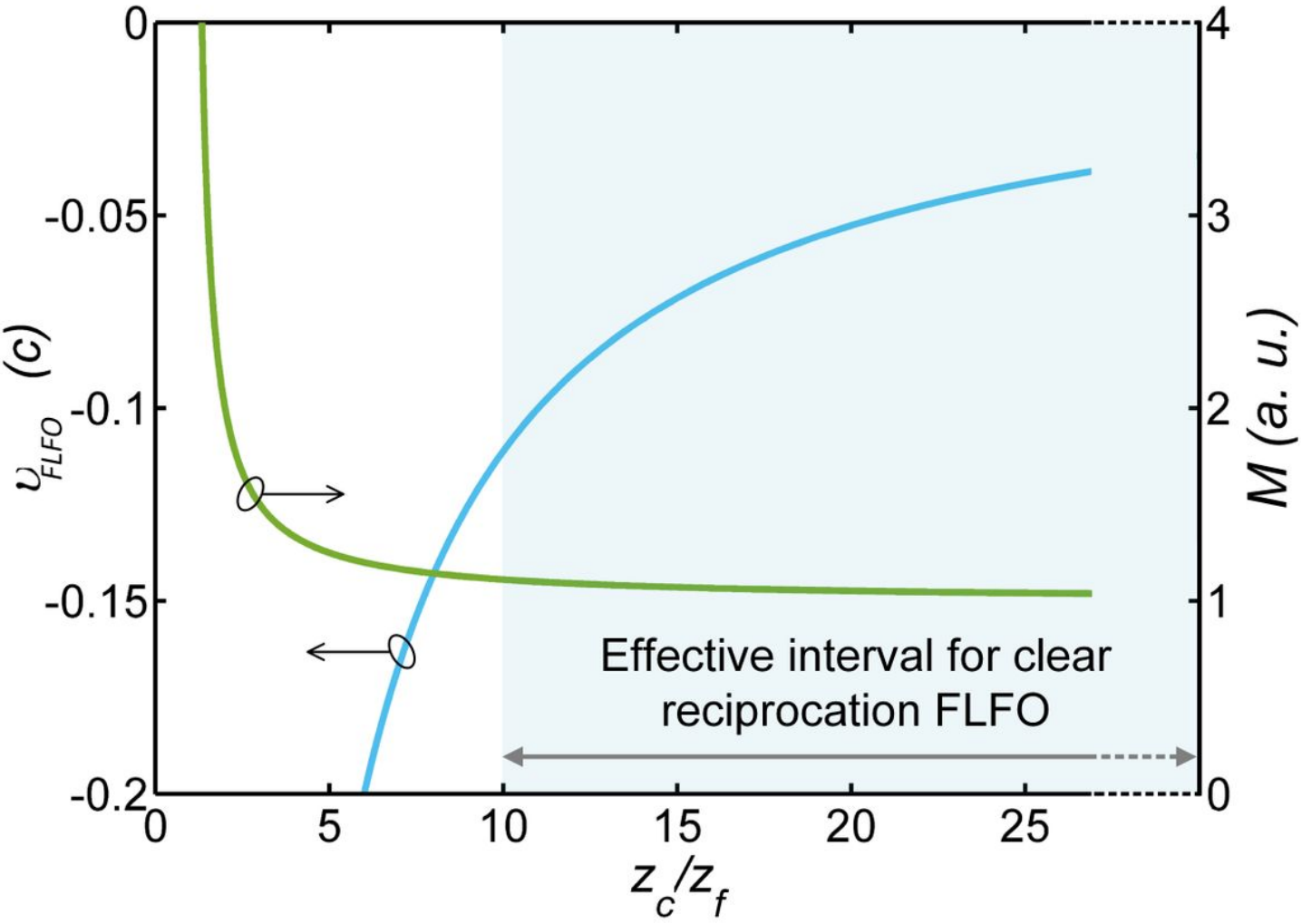

Figure 3

See manuscript for full figure caption.

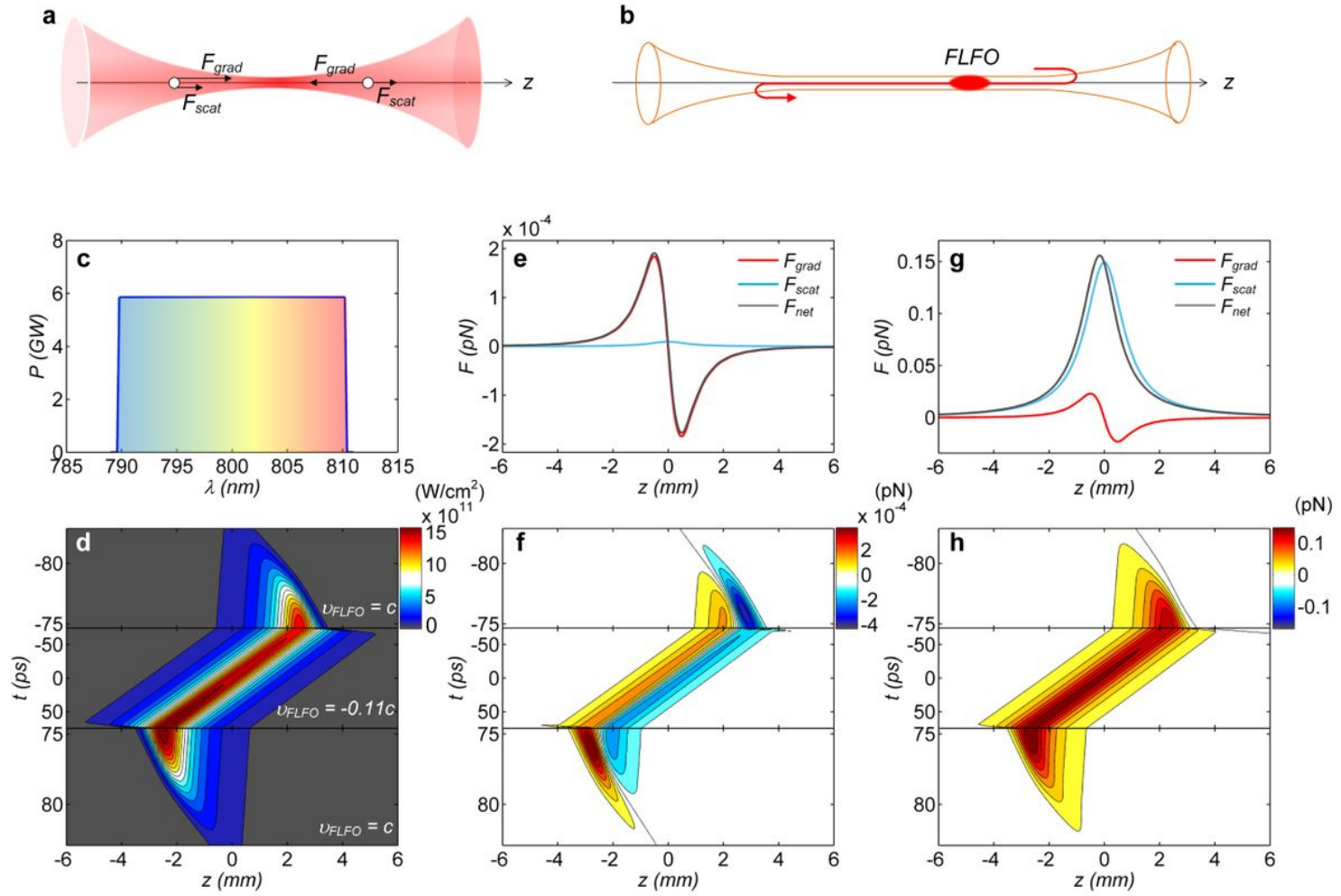

Figure 4

See manuscript for full figure caption.

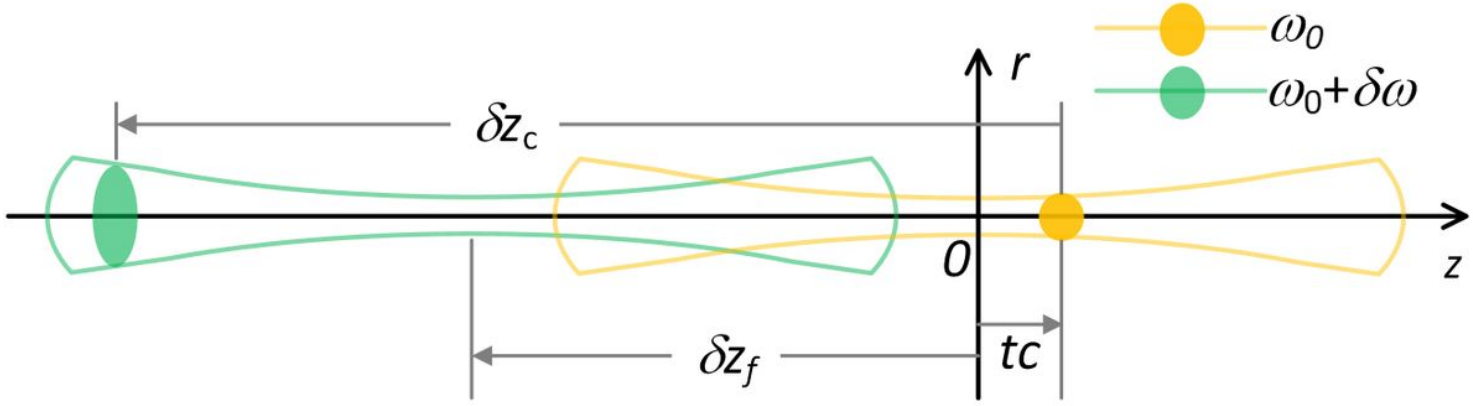

Figure 5

See manuscript for full figure caption.